

Chapter 4

Spin-Polarized Atoms in a Circularly Polarized Optical Dipole Trap

4.1 Introduction

Many precision measurements require spin-polarized neutral atoms and would be improved with trapped samples. However, no trap provides the necessary characteristics: atomic spin-polarization, tight confinement, ease of control, and a low photon-scattering rate. An imbalanced magneto-optical trap (MOT) has some modest polarization [65], and small spin-polarized samples have been maintained with repeated optical pumping cycles in standard dipole traps [66]. Magnetic traps can confine spin-polarized samples, and offer the advantage of RF transitions between non-degenerate Zeeman states that can be used to drive a variety of cooling schemes, including evaporative cooling and gravitational Sisyphus cooling [67, 45]. Unfortunately, magnetic traps have relatively weak spring constants, and strong magnetic fields are often undesirable and difficult to rapidly control. In contrast, an optical far-off resonance trap (FORT) [38, 39] offers superior confinement and rapid control. As noted in Ref. [43], a dipole trap made with circularly polarized laser light offers all the advantages of an optical trap, plus energy splittings between spin states that make cooling schemes possible in an inherently spin-polarizing trap. In this chapter, we report the creation of such a spin-polarizing FORT for Rb atoms using circularly polarized light.

4.2 Theory

A conventional FORT consists of a linearly polarized laser beam focused to a tight waist [38, 39]. Due to a spatially varying AC Stark shift, laser light tuned below an atom's resonant frequency attracts the atom to regions of high intensity. For alkali atoms in linearly-polarized light fields, the potential is the same for all internal spin states of the atom in the ground n ($S_{1/2}$) electronic state¹. This degeneracy is lifted when the light is circularly polarized; the laser field acts as a “fictitious magnetic field” [42]. When the laser is tuned between the D_1 ($n S_{1/2} \rightarrow n P_{1/2}$) and D_2 ($n S_{1/2} \rightarrow n P_{3/2}$) transitions, the energy splitting between the spin states is largest (Fig. 4.1). Also, the absorption of the circularly polarized FORT photons optically pumps the atoms into the deepest potential of the $F = 3$ manifold, shown for σ_+ polarization in Fig. 4.2.

¹ This is true if the laser detuning is much larger than the hyperfine splitting.

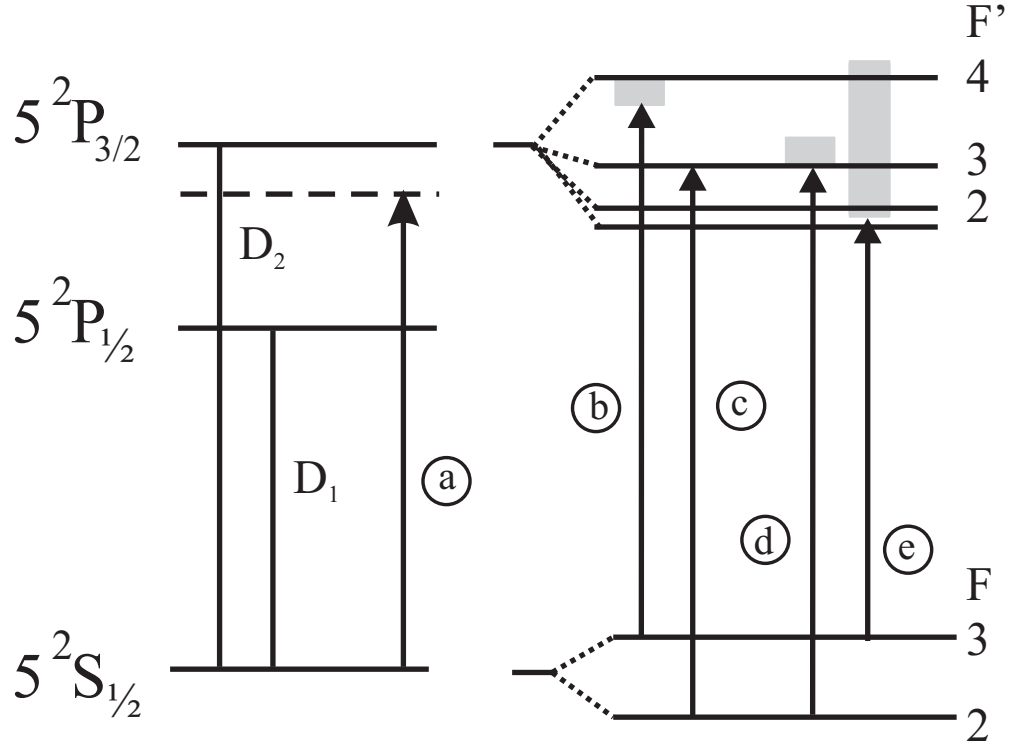


Figure 4.1: Schematic level diagram for ^{85}Rb ($I=5/2$). Laser beams are identified in the text as (a) FORT at 784.1 nm, (b) MOT cooling, (c) MOT repump, (d) transfer, and (e) probe. In vacuum, $\lambda_{D_2} = 780.2$ nm, $\lambda_{D_1} = 795.0$ nm [68].

The potential energy of atoms in an elliptically polarized FORT may depend on the laser polarization vector $\hat{\epsilon} \equiv 1/\sqrt{2}(\hat{x}\sqrt{1+\epsilon} + i\hat{y}\sqrt{1-\epsilon})$, with ϵ the ellipticity.² The potential depth $U_0(I, \lambda, F, m_F, \epsilon)$ is then

$$U_0 = \frac{\hbar\gamma I_0}{24I_S} \left[\left(\frac{1}{\delta_{\frac{1}{2}}} + \frac{2}{\delta_{\frac{3}{2}}} \right) - g_F m_F \sqrt{1-\epsilon^2} \left(\frac{1}{\delta_{\frac{1}{2}}} - \frac{1}{\delta_{\frac{3}{2}}} \right) \right] \quad (4.1)$$

where the natural line width $\gamma = 2\pi \cdot 6.1$ MHz in Rb, m_F is the Zeeman sublevel of the atom, $g_F = [F(F+1) + S(S+1) - I(I+1)]/[F(F+1)]$, the saturation intensity $I_S = 2\pi^2 \hbar c \gamma / (3\lambda^3)$, and the intensity $I_0 = 2P/(\pi w_0^2)$ in terms of power P .³ The detunings $\delta_{1/2}$ and $\delta_{3/2}$ (in units of γ) represent the difference between the laser frequency and the D_1 and D_2 transition frequencies, respectively. Figure 4.3 shows U_0 versus the laser wavelength for each m_F level. The potentials are described in terms of the Gaussian beam waist w_0 by

$$U(\rho) = U_0 \exp(-2\rho^2/w_0^2), \quad (4.2)$$

² ϵ is measured by rotating an analyzing polarizer in the laser beam and recording the highest and lowest power (P_h and P_l) transmitted through the analyzer. Then $\epsilon = (P_h - P_l)/(P_h + P_l)$.

³ Equation (4.1) is obtained by rewriting the expression for U_{AC} in Ref. [43] in terms of experimentally accessible quantities. For $\epsilon = 1$, Eq. (4.1) agrees with the expressions for U_0 in Ref. [69].

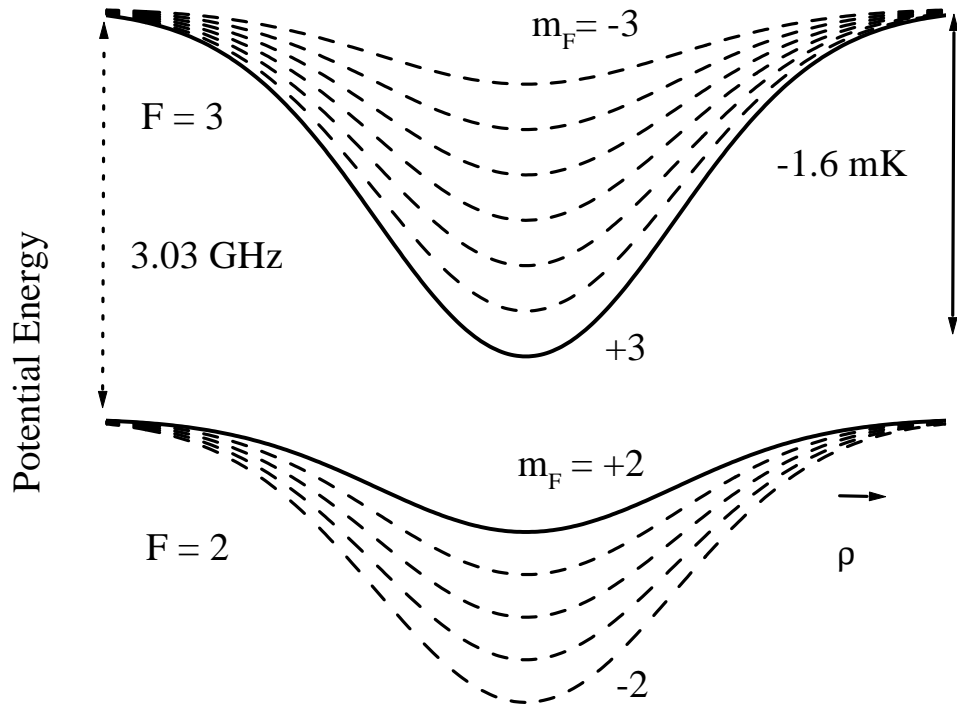


Figure 4.2: AC Stark shift $U(\rho)$ in the focus of a circularly polarized Gaussian laser beam for both hyperfine levels in the $^{85}\text{Rb } 5^2\text{S}_{1/2}$ ground state ($g_3 = 1/3$) under typical experimental parameters, for $P = 240$ mW. Solid lines indicate the spin states toward which the atoms are driven by absorption of the trapping light.

where $\rho = \sqrt{x^2 + y^2}$ is the radial spatial coordinate. Radial cross-sections of these potentials for ^{85}Rb are plotted in Fig. 4.2.

4.3 Experimental Setup

4.3.1 The Lasers

The experimental apparatus is shown in Fig. 4.4. The MOT [14, 15] collects Rb atoms from a 5×10^{-10} torr vapor, and contains a maximum of $\sim 3 \times 10^8$ atoms in steady state with a filling time constant of ~ 12 s. The MOT is made with two external-cavity diode lasers stabilized to atomic lines in Rb at 780 nm with a dichroic atomic vapor laser lock (DAVLL) (See Ref. [70] and Appendix A), which allows rapid and convenient tuning over > 100 MHz range. One laser, the “cooling” laser, provides 6 mW (divided between three retro-reflected beams) and is tuned to $5^2\text{S}_{1/2} F = 3 \rightarrow 5^2\text{P}_{3/2} F' = 4$. A second laser, the “repump” laser, is tuned to $5^2\text{S}_{1/2} F = 2 \rightarrow 5^2\text{P}_{3/2} F' = 3$. Both the cooling and repump lasers pass through acoustooptical modulators (AOMs) to control their power.

The dipole trap with adjustable polarization is created from up to 1 W of laser

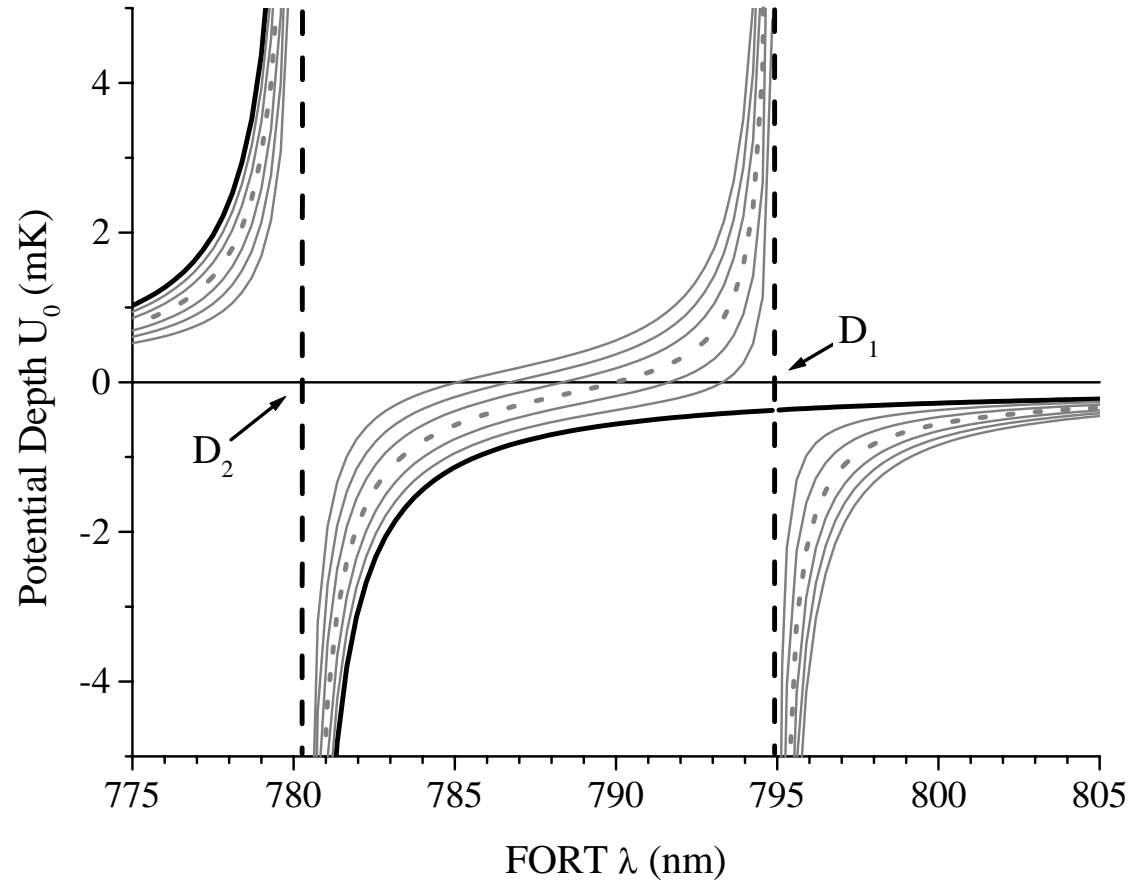


Figure 4.3: Maximum FORT Potential depth as a function of FORT wavelength, for the $F=3$ manifold with the following laser parameters; $P = 600$ mW, $w_0 = 26 \mu\text{m}$. The darkest line indicates the potentials for $m_F = +3$, into which the atoms are optically pumped by the FORT beam. The dashed line indicates the potential for atoms in the $m_F = 0$ state, which are insensitive to polarization.

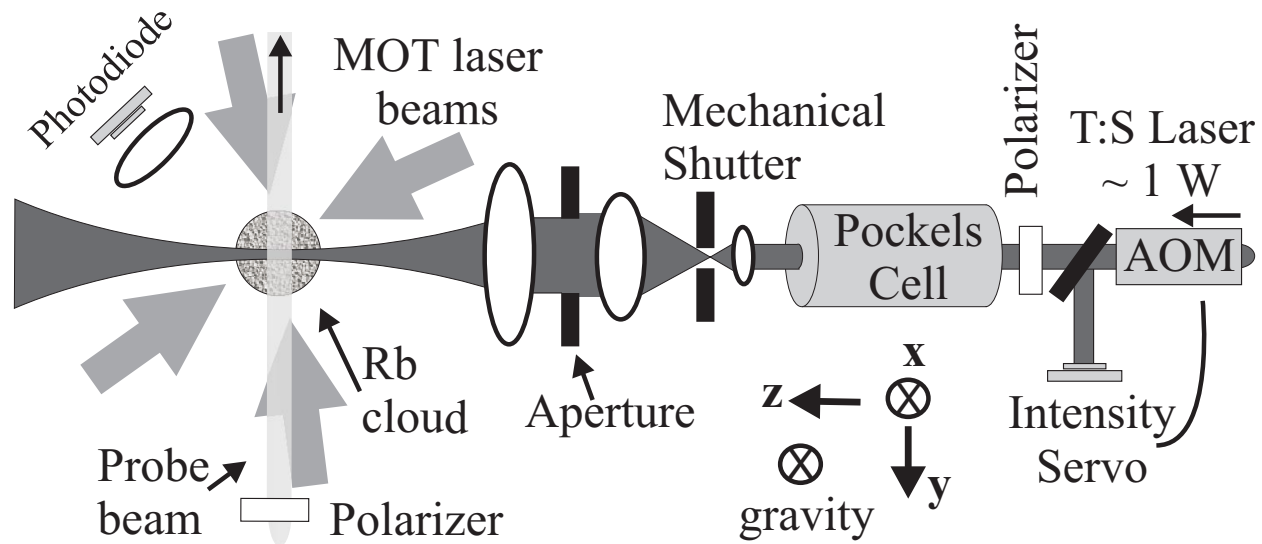


Figure 4.4: Schematic of the experimental apparatus. A “transfer” laser, not shown, counter-propagates with the FORT laser. Also not shown, a two-mirror periscope after the aperture elevates the FORT laser beam and turns it 90°. (See text.)

light from a Titanium:Sapphire laser, typically tuned to 784.1 nm. The laser beam passes through an AOM and the output power in the first diffraction order (70%) is usually actively stabilized to prevent parametric heating in the trap[71]. This beam passes through a Glan-Thompson polarizer and into a Pockels cell, which acts as a quarter-wave retarder when the applied voltage is about 2200 V. This voltage can be switched in a matter of 100 ms using a Hg relay. A mechanical shutter follows that can turn the FORT off in $60\mu\text{s}$. Finally the FORT beam ($w_0 = 4.2\text{ mm}$) is incident on an aperture and then a cemented doublet ($f = 18\text{ cm}$) that focuses it to $w_0 = 26\ \mu\text{m}$.

The FORT laser beam waist w_0 is measured by inserting a mirror after the doublet lens such that the FORT laser comes to a focus outside the chamber. A razor blade is then translated across the beam while monitoring the position of the blade x and the amount of power that is not blocked by the razor blade $P(x)$. The resulting data are fit to the following function $P(x) = P_{\text{max}}/2[1 \pm \text{erf}(\sqrt{2} \times (x - x_c)/w)]$ to determine the width w of the beam. This measurement was repeated at many longitudinal positions until the narrowest waist w_0 was found. By examining the dependence of w on z , the effective Rayleigh range could be found. This often exceeded the Rayleigh range calculated from w_0 using Gaussian optics [72] by as much as a factor of 3, perhaps due to aberrations in the lens.

4.3.2 The Pockels Cell and Polarization Issues

Establishing the proper polarization of the laser using a Pockels cell requires precision and patience. As will be shown later, a very well-defined polarization is essential to the performance of the circular FORT. This requires careful alignment of the Pockels cell. Our Pockels cell comes from Cleveland Crystals, model number Q1020S. As with all Pockels cells, it relies on the Pockels effect [73], which is a birefringence induced in a crystal that is proportional to the applied voltage. This linear effect is present only in crystals that lack a center of symmetry, such as KDP and KD*P.

To align the Pockels cell, first two crossed polarizers are aligned in the FORT beam such that the first polarizer gives maximum transmission and the analyzer provides extinction. Next, the Pockels cell is inserted in the beam between the polarizers and a large voltage (approximately the $\lambda/2$ voltage if safely possible) induces birefringence. Then the cell is rotated until extinction is again observed after the analyzer. This establishes that the “fast axis” of the cell is aligned with the incident polarization. The cell is then rotated such that the fast axis is at a 45° angle with respect to the incident polarization. The applied voltage is reduced to nearly the nominal $\lambda/4$ value and then adjusted until $\lambda/4$ voltage is obtained, and the polarization is as nearly circular as possible. Figure 4.5 shows the measured polarization ellipticity as a function of applied voltage.

The angle that the cell’s longitudinal axis makes with the laser’s direction of propagation is also important. One alignment trick is to place a piece of cellophane tape across the input port of the Pockels cell. This creates diffuse, unpolarized scattered light at the input, some of which passes through the Pockels cell. If a piece of paper is placed along the beam path after the analyzing polarizer, the diffuse light forms a large round

spot. When the Pockels cell has a large applied voltage, a cross-shaped interference pattern appears in the diffuse spot when it is viewed through the analyzing polarizer. By tilting and translating the Pockels cell, this cross shape can be centered within the diffuse spot. The incoming laser beam, when not passing through the transparent tape, should also strike the center of the cross. To perform this alignment, it is necessary to insert and remove the transparent tape repeatedly.

By iteratively rotating, tilting, and translating the Pockels cell, optimum alignment can be obtained, in which the light can be switched from completely linear to completely circular by changing the applied voltage. However, after the Pockels cell a periscope composed of two mirrors is required to elevate the beam so that it can enter the vacuum chamber. This presents a problem because mirrors induce large, angle- and polarization-dependent phase shifts in reflected beams, they are therefore not in general polarization-preserving. However, the polarization can be preserved by using two gold-coated mirrors each of which reflects the beam at right angles such that the final beam is above and perpendicular to the incoming laser beam. By monitoring the polarization after the periscope and the vacuum chamber, small changes in the periscope alignment can be used to optimize the polarization. Residual phase shifts in circular light induced by the periscope can also be compensated by the Pockels cell voltage, as in Fig. 4.5. Any time the alignment of the laser through the periscope changes, one must verify the $\lambda/4$ voltage. In measuring the beam polarization, one must use high-quality polarizers such as calcite Glan-Thompson polarizers. It is also important to use the entire laser beam when measuring the polarization, because both the periscope and the Pockels cell can introduce non-uniformity in the polarization that can limit the lifetime of the atoms in the circular FORT.

4.3.3 Diagnostics and Loading

The number and lifetime of atoms in the FORT are characterized using the following timing sequence. The MOT is allowed to fill for some time τ_f before the atoms are transferred from the MOT into the FORT. They are then stored in the FORT in the absence of any other light sources or the quadrupole magnetic field for some time τ_S . To detect the atoms, the FORT is turned off and the MOT quadrupole magnetic field remains off while the MOT cooling and repump lasers are turned on again, tuned closer to resonance ($-\gamma/2$). The number of atoms N is then inferred from the measured fluorescence [74] and plotted as a function of τ_S (Fig. 4.6). The decay in N is governed by the differential equation

$$\dot{N} = -\Gamma N - \beta' N^2, \quad (4.3)$$

where Γ describes exponential loss processes involving a single trapped atom and β' characterizes the density-dependent losses. The prime on β' is used to refer to atom number loss, instead of density loss. The data are fit to the solution [75]

$$N = N_0 e^{-\Gamma t} / [1 + (\frac{\beta' N_0}{\Gamma})(1 - e^{-\Gamma t})], \quad (4.4)$$

as shown in Fig. 4.6. From this fit, the initial number N_0 , Γ , and β' are extracted.

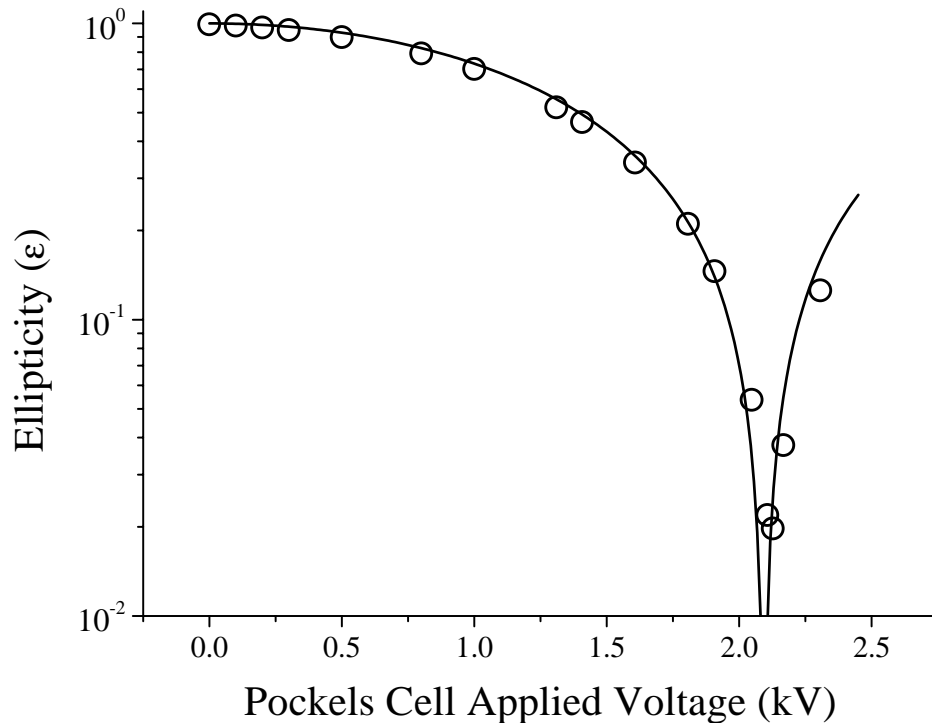


Figure 4.5: Characterization of FORT laser beam polarization after Pockels cell and periscope, as a function of the voltage applied to the Pockels cell. Ellipticity is described in Section 4.2. The black line represents a fit to $\epsilon = |\cos^2(\pi/4(V/V_R) - \sin^2(\pi/4(V/V_R))|$, where V_R is the desired reference voltage that provides perfectly circular light after the periscope.

The physics involved in the transfer of atoms from the MOT to the FORT is quite complicated and will be discussed elsewhere (See Ref. [44] and Chapter 5). Here, we give a summary of results. For the parameters in Fig. 4.6, simple “geometrical loading,” in which the FORT laser is turned on immediately after the MOT turns off, traps about 2×10^5 atoms. N_0 can be increased by leaving the MOT on with different detuning and power parameters while the FORT is loading. This increase indicates that the MOT lasers cool atoms as they fall into the FORT. For the same FORT parameters, the best loading is typically achieved by detuning the cooling laser to -5γ and reducing the intensity of the hyperfine pump to $10 \mu\text{W}/\text{cm}^2$ for 70 ms before the MOT lasers and magnetic fields are switched off. This procedure transfers up to 20% of the MOT atoms into the FORT.

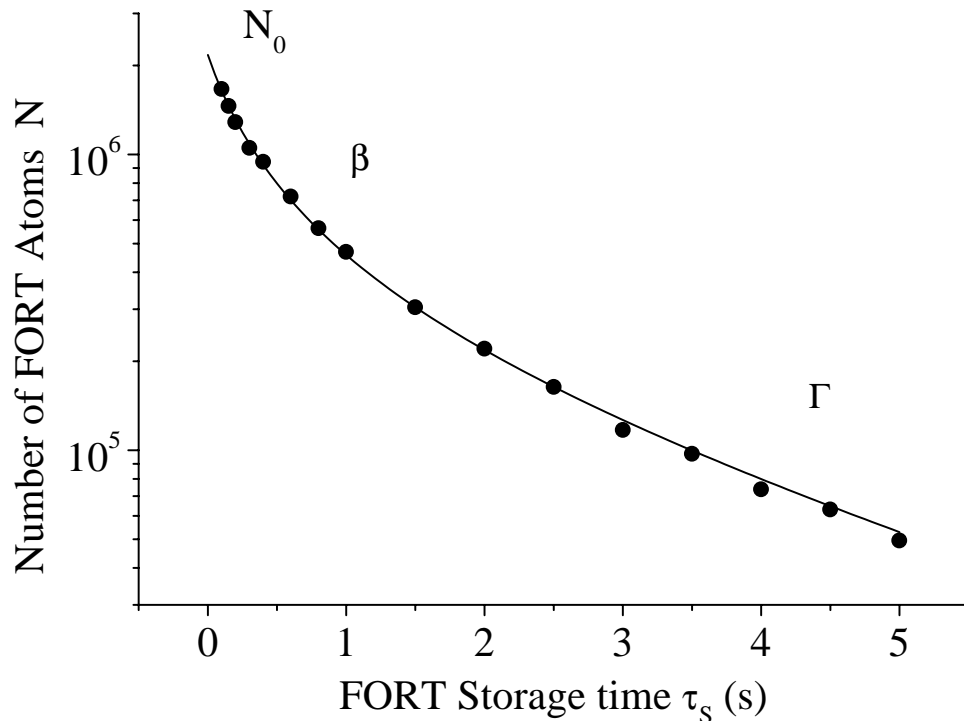


Figure 4.6: Number of atoms stored in a linearly polarized FORT ($U_0 = -1.8$ mK at 540 mW) as a function of trapping time, after filling the MOT for $\tau_f = 1$ s. No data is taken for the first 100 ms while the MOT atoms fall away. The solid line is a fit to Eq. (4.4), giving $N_0 = 2.2 \times 10^6$ atoms, $\beta' = 1.3 \times 10^{-6}$ (atoms s) $^{-1}$, and $1/\Gamma = 3.0$ s. For $\tau_f = 4$ s, 4×10^6 atoms are initially trapped in the linear FORT.

4.4 The Elliptically and Circularly Polarized FORTs

4.4.1 Loading Atoms into the Circular FORT

Optimum loading into an elliptically polarized FORT ($\epsilon < 1$) is different from simply loading into the linear FORT. While geometrical loading still gives similar numbers, only about half as many atoms can be loaded using MOT cooling. The most efficient way to transfer atoms into an elliptical FORT is to first load the linear FORT, and then use the Pockels cell to quickly change the polarization from linear to the desired polarization. This procedure transfers about 70% of the atoms originally held in the linear FORT, regardless of the time constant that governs the change in polarization (from 0.2 to 20 ms). Up to 100% of the atoms in the linear FORT are transferred to the circularly polarized FORT (“circular FORT”) by a “transfer” laser beam, circularly polarized and aligned anti-parallel to the FORT laser. This beam, tuned to the $5^2S_{1/2} F = 2 \rightarrow 5^2P_{3/2} F'$ transition, is applied for 20 ms after the FORT polarization changes to circular. When σ_+ -polarized, this transfer beam assists the FORT in optically pumping the atoms into positive m_F levels, and tends to keep them in the $F=3$

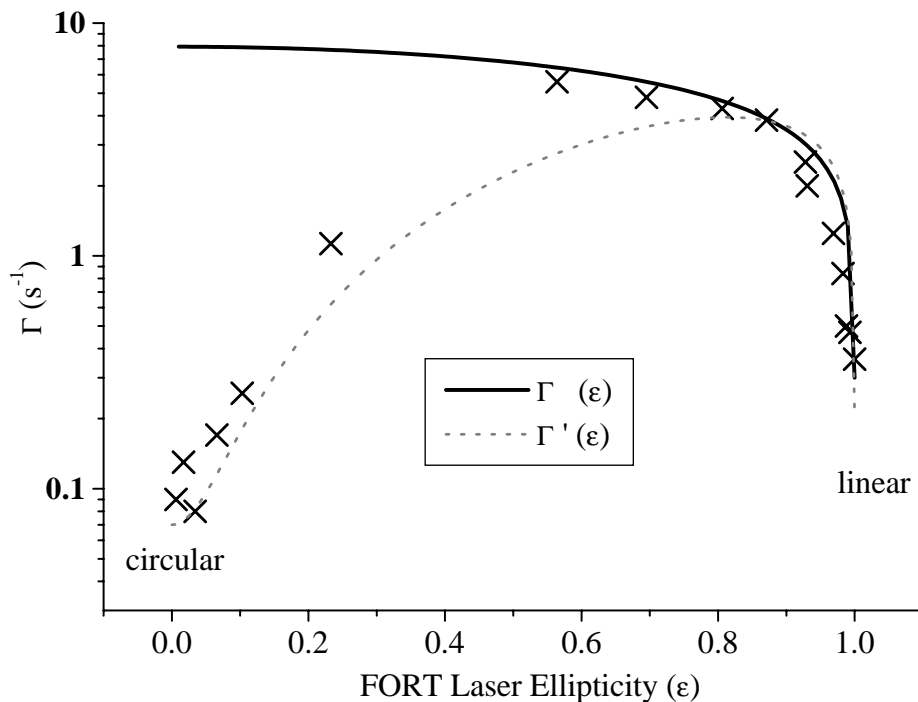


Figure 4.7: Dependence of the FORT exponential loss rate Γ on the ellipticity ϵ of the FORT laser polarization. Crosses indicate the measured loss rate, which is small for purely linear ($\epsilon = 1$) and purely circular ($\epsilon = 0$) polarizations. Because the circular potentials are deeper as indicated in Fig. 4.2, $\Gamma(\epsilon = 0) < \Gamma(\epsilon = 1)$. $P = 280$ mW, $U_0(m_F = 0) = -0.77$ mK, and $U_0(m_F = +3, \epsilon = 0) = -1.5$ mK. The solid and dashed curves represent models of the ground-state dipole-force fluctuation heating described by Eq. (4.5), plus a small offset due to collisions with the background vapor.

states. Thus atoms are pumped to the deep $F = 3, m_F = +3$ potential whence they are not readily lost. In this fashion, 4×10^6 atoms were loaded into a circular FORT at $\lambda = 782.3$ nm with $U_0(m_F = 0) = -2.0$ mK.

4.4.2 Elliptically Polarized FORT Decay Rates

The lifetime τ of the FORT depends dramatically on the polarization of the FORT laser. A measurement of the decay rate $\Gamma = 1/\tau$ as a function of the ellipticity ϵ of the FORT laser polarization is shown in Fig. 4.7. Γ is smallest when the polarization is perfectly linear or perfectly circular. In addition, Fig. 4.8 shows how Γ changes with FORT intensity for each of these polarizations. Above a trap depth of about $U_0 = -0.2$ mK, the decay rate is independent of intensity for both linear and circular light, but increases linearly with FORT intensity for an intermediate elliptical polarization.

The large losses at imperfect polarizations are due to ground-state dipole-force

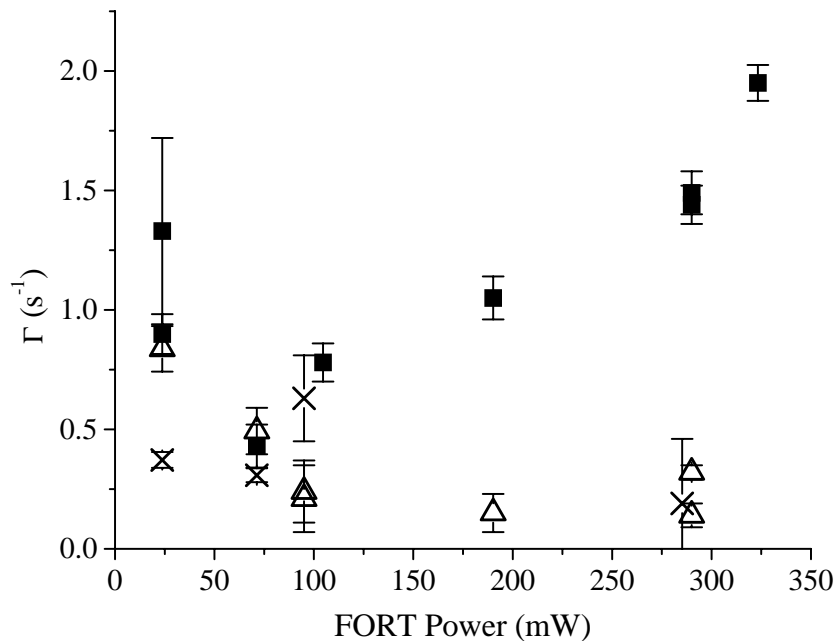


Figure 4.8: Exponential decay rate Γ vs. FORT peak intensity for three different FORT polarizations: linear (\times , $\epsilon = 99.995\%$), circular (Δ , $\epsilon = 0.6\%$), and elliptical (\blacksquare , $\epsilon = 21\%$). FORT $\lambda = 784.2$ nm, $w_0 = 31$ μ m, and the maximum $U_0 = -0.8$ mK for linear polarization at 330 mW.

fluctuation heating that arises when atoms change internal spin state [10]. In the linear FORT, all the ground-state potentials are degenerate, so there is no heating associated with changing the ground level m_F state. However, when the polarization is elliptical, these levels are no longer degenerate, and changes between the levels cause instantaneous changes in the dipole force acting on the atom. These changes result in heating, which evaporates atoms from the trap. The heating rate depends on the rate at which the atoms change state, which in turn depends on the FORT scattering rate. Therefore this heating mechanism increases linearly with intensity. In the circular FORT, however, only $\Delta m_F = +1$ transitions can be excited, and the atoms are all pumped into the $F = 3$, $m_F = +3$ state in about 30 ms. After that, they no longer change their ground state and this heating process turns off.

4.4.3 Model of Lifetime vs. Ellipticity

Agreement between the data and a simple model supports this picture. The dependence of heating on FORT polarization can be modeled with a two-level system using the two trapping potentials of the $5^2S_{1/2}$ $F = 3$, $m_F = +3$ and $F = 2$, $m_F = +2$

states, labeled $|a \rangle$ and $|b \rangle$. These states are selected because the U_0 for each is very different, and yet they are closely coupled via off-resonant excitation by the FORT beam. We approximate the potentials as harmonic. Atoms initially held in $|a \rangle$ spread out when they are transferred to $|b \rangle$, which has a smaller spring constant, and then heated when they re-enter $|a \rangle$ with a larger spatial extent and therefore more potential energy. Assuming the atoms hop between the two potentials at a constant rate Γ_h , we derive the exponential time constant as a function of FORT ellipticity:

$$\Gamma(\epsilon) = \Gamma_h \ln \frac{U_a(\epsilon)}{U_b(\epsilon)} / \ln \frac{T_f}{T_i}, \quad (4.5)$$

where $U_a(\epsilon)$ and $U_b(\epsilon)$ are calculated for states $|a \rangle$ and $|b \rangle$ using Eq. (4.1), and T_i and T_f are the initial and final temperatures, chosen to be $100 \mu\text{K}$ and U_0/k_B , respectively. As shown by the solid curve in Fig. 4.7, Eq. (4.5) explains the rapid decrease in Γ as ellipticity approaches linear, but does not fit well near circular.

The decrease in Γ near circular polarization arises from a dependence of the hopping rate on FORT ellipticity. Because the system actually contains many hyperfine and spin states, it is difficult to model exactly. A simplified approach assumes that absorption of a σ_- photon causes transfer from $|a \rangle$ to $|b \rangle$ and absorption of a σ_+ photon transfers atoms back to $|a \rangle$. This gives a new rate of hopping between potentials $\Gamma'_h = \epsilon^2 \Gamma_h$ and modifies the expression for the exponential heating rate in the trap to be $\Gamma'(\epsilon) = \epsilon^2 \Gamma(\epsilon)$. Figure 4.7 shows fits to both $\Gamma(\epsilon)$ and $\Gamma'(\epsilon)$, with Γ_h the only free parameter in each case. They yield $\Gamma_h = 13/\text{s}$ and $\Gamma_h = 17/\text{s}$, respectively. To calculate an optical scattering rate from these values, we simply divide by the product of the appropriate Clebsch-Gordan coefficients (0.05) for the four-photon heating process (absorption, emission to $F = 2$, absorption, emission to $F = 3$). The resulting scattering rates (260/s and 340/s) agree well with the estimated average scattering rate in the FORT to within its 50% uncertainty.

4.4.4 FORT $\lambda > \lambda_{D_1}$

The decay of atoms from the FORT behaves very differently depending on the wavelength of the FORT laser light. All the data preceding and following this section were taken with the FORT wavelength smaller than 795 nm. In these cases, the circular FORT decay curves fit well to Eq. (4.4). In contrast, when the circular FORT wavelength is red of both the D_1 and D_2 transition, Fig. 4.9 shows that the decay of atoms occurs over two very different exponential time scales. In Fig. 4.9, (■) are fit to

$$N = A_1 e^{-t/\tau_1} + A_2 e^{-t/\tau_2} \quad (4.6)$$

yielding $\tau_1 = 65 \pm 8 \text{ ms}$ and $\tau_2 = 3.2 \pm 0.2 \text{ s}$. Time constant τ_2 comes from the same background collisional loss rate observed in the decay of atoms from the CFORT tuned between the D_1 and D_2 lines, and in the linear FORT. However, the new, faster decay rate τ_1 is due to optical pumping and evaporative loss of atoms by the circular FORT.

Optical pumping of atoms in the circular FORT only causes additional losses when the FORT is tuned red of the D_1 transition. In this case, the sign of the second

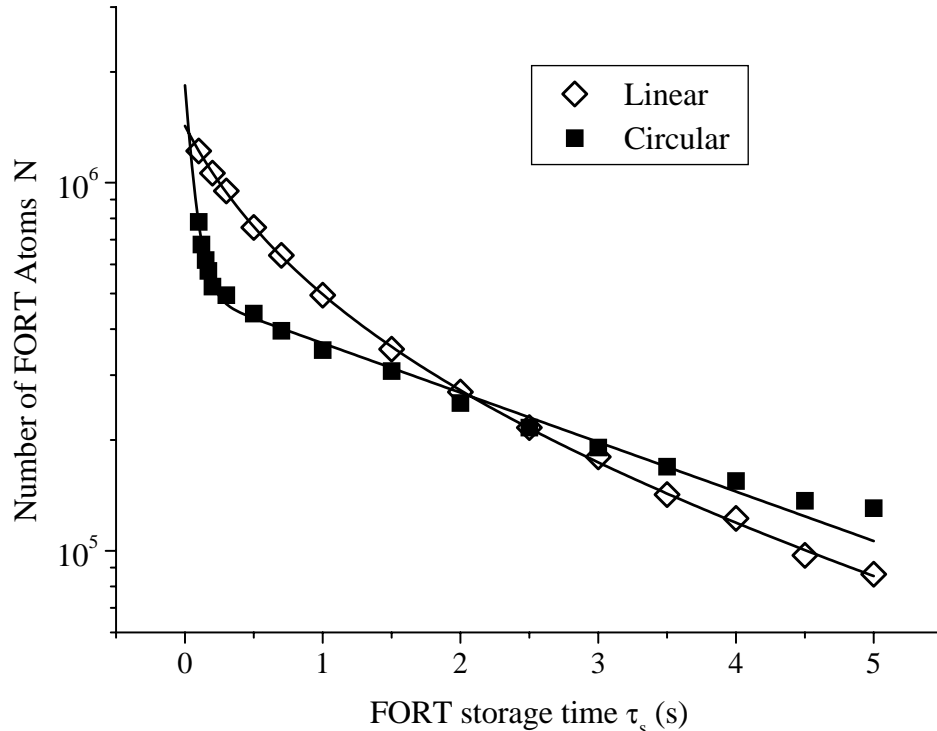


Figure 4.9: FORT decay curve with FORT $\lambda = 798.4$ nm, $P = 290$ mW, and $w_0 = 31$ μm for both linear (\diamond , $U_0 = -0.7$ mK) and circular [\blacksquare , $U_0(m_F = +3) = -0.3$ mK] polarizations. Solid lines represent fits to Eq. (4.4) and Eq. (4.6) respectively.

term of Eq. (4.1) is such that the circular FORT tends to optically pump atoms into the shallowest potential. Measurements described in the next chapter (Section 5.5) indicate that the FORT holds the temperature of the atoms at $T = 0.4 \times U_0/k_B$. Therefore, atoms initially held in the linear FORT have temperatures too large to be confined in the shallower potentials of the circular FORT once they are pumped into them. Atoms initially in the $m_F = 3$ state evaporatively cool until they can be held by the shallow potential. In addition, atoms in the deeper states are optically pumped into the shallowest state, and also evaporatively cool. Once all the atoms are optically pumped and have evaporated to a reasonable temperature, this source of loss ceases to contribute to the decay in the number of atoms.

Brief attempts to minimize the losses due to optical pumping were unsuccessful. These included varying the time over which the polarization was switched, and using the circularly-polarized “transfer beam” to optically pump the atoms before the potential is switched. Neither of these can eliminate the essential problem: atoms originally held in the linear FORT have too much kinetic energy to be retained by the shallower $F = 3$, $m_F = 3$, regardless of how they make the transition. One technique that may work well is to reduce the linear FORT power to some fraction f of maximum at the beginning of the cycle, where f is the ratio between $U_0(m_F = 3)$ and $U_0(m_F = 0)$;

$f = 2$ at FORT $\lambda = 800.0$ nm. Then one should apply the transfer beam to optically pump most of the atoms into the $F = 3, m_F = 3$ state, and then simultaneously restore the FORT power to its maximum value and turn on the Pockels cell. In this way, the depth of the well containing the atoms would not change, and evaporative losses could be eliminated.

4.5 Spin-Polarization Demonstration

The inherent spin-polarizing nature of the circular FORT is confirmed by measuring the fraction of atoms that populate the $F = 3, m_F = +3$ state. Exciting the atoms in the $F = 3$ state with an additional laser causes loss by pumping them to the weakly trapped $F = 2$ state. We compare the loss when all m_F states are excited to the loss when all but $m_F = +3$ is excited. The probe laser beam (Figs. 4.1 and 4.4) is linearly polarized and tuned to excite ${}^2S_{1/2} F = 3 \rightarrow {}^2P_{3/2} F'$ transitions. When this beam is aligned as shown in Fig. 4.4, it induces either $\Delta m = 0$ or $\Delta m = \pm 1$ transitions, depending on whether the polarization is oriented horizontally or vertically. The probe beam is pulsed on for 20 ms at an intensity of $1 \mu\text{W}/\text{cm}^2$, 45 ms after the MOT is switched off. We then measure the resulting decrease in the number of atoms in the circular FORT. This signal is plotted as a function of frequency in Fig. 4.10 for both polarizations. When the laser is tuned to the $F = 3 \rightarrow F' = 2$ transition and the polarization is vertical (\bullet), we find that the loss saturates at 33%. However, when the polarization is horizontal (\diamond), unsaturated loss is only 4%. The difference in fractional loss indicates a large population in the $m_F = +3$ state, because horizontal polarization does not excite atoms in this state, while vertical excites all spin states. After including a factor of 2 for saturation, the ratio of the two losses implies that 7% of the atoms are not in the $F = 3, m_F = +3$ stretched state. Because these atoms are most likely to be in the $m_F = +2$ state, the spin-polarization is 98(1)%.

4.6 Conclusion

We have demonstrated and characterized a circularly polarized FORT. We have also shown that the trap provides a high degree of spin-polarization. The splittings of m_F levels in the circular FORT should allow RF cooling techniques in the trap similar to methods employed in magnetic traps. Finally, we have shown that small polarization imperfections in circular or linear FORTs can lead to heating and subsequent loss due to ground-state dipole-force fluctuations.

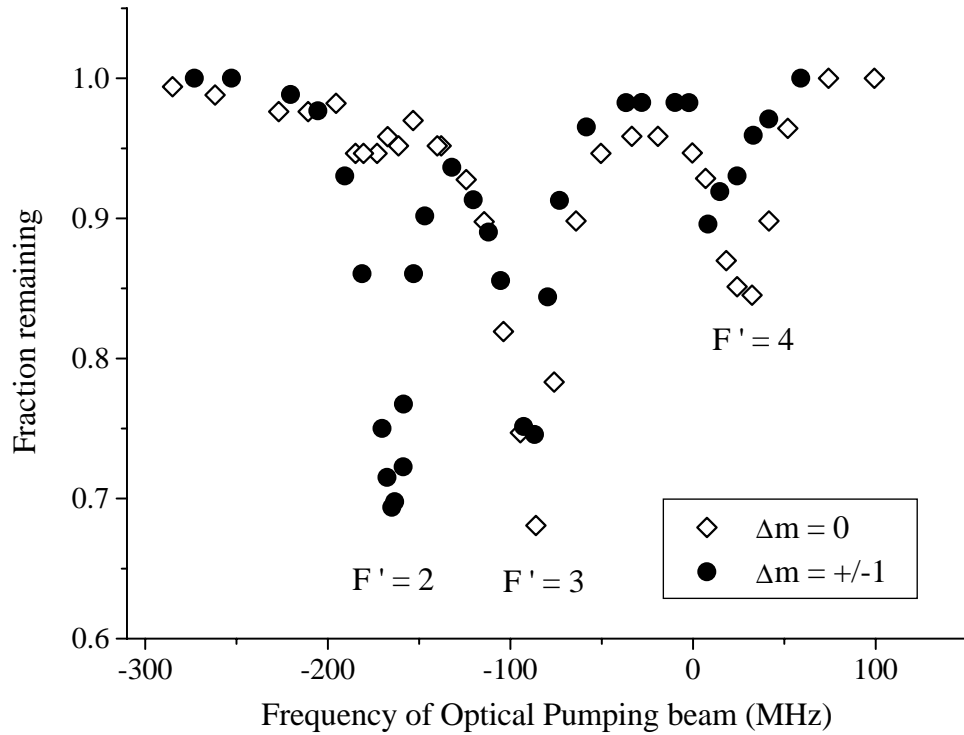


Figure 4.10: Fraction of atoms remaining in the FORT as a function of the frequency of an applied optical pumping beam for two different polarizations: (\diamond and \bullet). Frequency is measured with respect to the frequency of the unshifted $5^2S_{1/2} F=3 \rightarrow 5^2P_{3/2} F'=4$ transition. Signals are normalized to the number of atoms held in the trap without the optical pumping beam (8×10^5 atoms). Resonances are AC Stark-shifted about 30 MHz with respect to the resonances in free atoms, and separations are consistent with the $5^2P_{3/2}$ hyperfine splitting. The difference between \diamond and \bullet for $F'=2$ is clear evidence for spin-polarization. This shallow trap [$P=190$ mW, $U_0(m_F=0) = -0.63$ mK, and $U_0(m_F=3) = -1.2$ mK] allows resolution of the hyperfine structure. In deeper traps, the spin-polarization should only improve.